Hyperfine splitting and isotope-shift measurements within the 378-nm $6P_{1/2}$-$7S_{1/2}$ transition in ^{203}Tl and ^{205}Tl

D. S. Richardson, R. N. Lyman, and P. K. Majumder
Department of Physics, Williams College, Williamstown, Massachusetts 01267
(Received 3 February 2000; published 15 June 2000)

Using a frequency-doubled diode laser system, we have measured the hyperfine splitting in the $(6s^2 7s)7S_{1/2}$ excited state of the two naturally occurring thallium isotopes. For ^{205}Tl and ^{203}Tl we find frequency intervals of 12294.5(1.5) and 12180.5(1.8) MHz, respectively. This measurement addresses an earlier discrepancy in measured values for these intervals. At the same time, we have measured, with a factor of 50 improved precision, the ^{205}Tl-^{203}Tl isotope shift within the 378-nm $6P_{1/2}$-$7S_{1/2}$ transition.

PACS number(s): 32.10.Fn, 31.30.Gs, 27.80.+w

I. INTRODUCTION

In recent years, the precision reached in parity nonconservation (PNC) experiments [1,2], coupled with advances in atomic theory of the relevant elements [3,4], has enabled new atomic-physics–based tests of the standard electroweak model. In thallium, a new round of atomic structure calculations has just been completed [5]. These calculations require a variety of independent atomic structure measurements of high precision to provide cross-checks on accuracy and guide the development of the theory. Recently, we completed a precise measurement of the electric quadrupole component amplitude [6] within the same 1283-nm $6P_{1/2}$-$6P_{3/2}$ transition in which PNC was measured [2]. Here we report a measurement of the hyperfine splitting (HFS) of the $7S_{1/2}$ excited state in the two naturally occurring thallium isotopes ^{205}Tl and ^{203}Tl. For this measurement we have utilized a frequency-doubled diode laser optical system at 378 nm. As part of this experiment, we have also made a direct, laser-based measurement of the isotope shift within this UV transition.

Measurements of hyperfine constants and isotope shifts offer complementary atomic structure information to that obtained from transition-amplitude or Stark-effect measurements in that they focus on the nature of the wave function near the nucleus. Since atomic PNC effects depend intimately on the behavior of the electron wave function near the nucleus, these HFS measurements can serve as very useful tests of the theory. Also, precise HFS measurements are useful as inputs to semiempirical calculations, such as those recently undertaken in thallium [4,5].

Microwave techniques were used in the 1950s to obtain highly precise (uncertainty less than 1 kHz) HFS measurements [7] in the $6P_{1/2}$ and $6P_{3/2}$ states of the thallium isotopes. In contrast to this situation, measurements of the $7S_{1/2}$-state HFS are far less precise, and show poor internal agreement. In particular, a 1990 measurement of the $7S_{1/2}$ HFS by Hermann *et al.* [8] was later corrected [9] by roughly 50 MHz ($\sim$13 standard deviations) due to apparent calibration and linearization errors. The newer values remain somewhat discrepant from 1985 work by Neugart *et al.* [10]. Section V of this paper discusses our results in the context of this previous work.

In addition to their relevance to the atomic theory of thallium, these measurements can provide important information concerning the thallium nuclei. The isotope shift between thallium 203 and 205 can be split into field and mass shift components. The field shift is proportional to the value of the electronic wave function at the origin as well as $\delta\langle r^2\rangle$, the change in the mean-square charge radius between the nuclei. Given atomic structure calculations of high precision, an accurate estimate of the latter quantity can be deduced [11]. Finally, hyperfine anomaly and isotope shift measurements can serve as tests of nuclear structure calculations. As pointed out in [12] and discussed in Sec. V below, models of nuclear magnetic moment distributions can be tested via measured hyperfine anomalies. Such a comparison may have implications for so-called ''Schiff moments'' used in interpretation of experiments measuring *P*- and *T*-violating effects, such as are ongoing in thallium [12,13].

II. EXPERIMENTAL DETAILS

Figure 1 shows the energy levels and relevant transitions of the thallium 378-nm transition for the two stable thallium isotopes ^{203}Tl and ^{205}Tl, each of which has nuclear spin $I = 1/2$. The spectrum consists of three pairs of transitions separated by large ground- and excited-state hyperfine splittings. The opposing isotopic level shifts of the relevant states produce a rather large $\sim$1.7 GHz transition isotope shift (TIS) at 378 nm, where TIS is defined as the frequency shift $\Delta\nu_{205\text{-}203}$ that would be observed for this transition in the absence of hyperfine structure. Even for the case of our Doppler-broadened vapor cell transmission signal (Doppler half-width $\sim$600 MHz), this shift is well resolved. Because of the significant isotopic differences in hyperfine splittings for both the thallium $6P_{1/2}$ and $7S_{1/2}$ levels, it is not possible to spectroscopically measure the isotope shift independent of the hyperfine splittings. In our case, we analyze our experimental spectra by parametrizing each of the observed splittings as the appropriate linear combination of IS and HFS. A particularly valuable feature of our spectroscopy experiment is the ability to tune the laser continuously over the roughly 40 GHz total extent of the ground- and excited-state hyperfine structure. Since the ground-state HFS has been previously measured to such high accuracy [7], this frequency splitting serves as an ideal absolute frequency calibration for

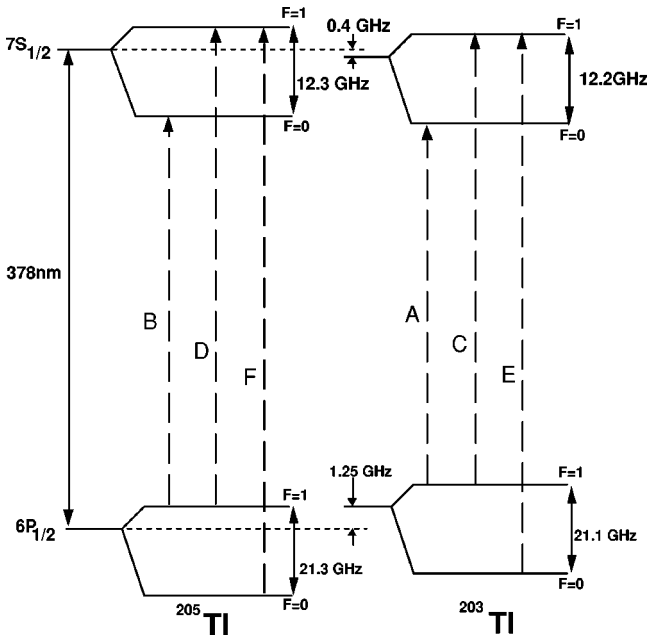

FIG. 1. Energy levels within the 377.6-nm $6P_{1/2}$-$7S_{1/2}$ transition in ^{203}Tl and ^{205}Tl. Level shifts are not to scale. The six lines are labeled A–F for identification on Fig. 3.

our measurement of the excited-state splittings and isotope shift.

The vapor cell oven interaction region used for this experiment has been described elsewhere [6], so the description here will focus on the optical system developed for this experiment. Referring to Fig. 2, we produce roughly 3 mW of infrared light at 755 nm via an external cavity diode laser (EOSI model 2010). A small portion of this light is simultaneously directed into a pair of low-finesse confocal Fabry-Pérot cavities. The differing free spectral ranges (FSRs) of these cavities (roughly 330 and 540 MHz, respectively) provide independent frequency calibration and interpolation as described below. Each cavity is contained in an insulating box for passive thermal stabilization. The shorter cavity is a commercial unit (Burleigh RC-110), while the second is of homemade design [14]. By comparing the location of the Fabry-Pérot transmission peaks relative to the atomic peaks in our experimental spectra taken over the course of many hours, we are confident that any possible frequency calibration errors due to thermal drift during a single scan are negligible compared to our final uncertainties. We also direct a small amount of infrared light to a wavemeter (Burleigh WA-1500) which is used both to set and monitor the exact laser frequency, and to calibrate the Fabry-Pérot cavity FSRs.

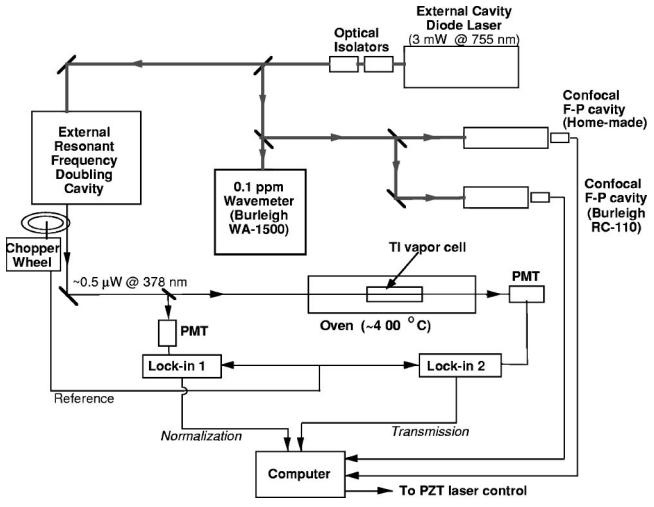

FIG. 2. Schematic diagram of the apparatus.

After passing through two consecutive optical isolators (total isolation greater than 50 dB), the main infrared beam is circularized using two cylindrical lenses and passed through an additional spherical lens to provide mode matching of the beam into an external resonant frequency-doubling cavity [15]. The four-mirror ''bowtie'' configuration of this cavity includes two spherical focusing mirrors with a lithium triborate doubling crystal located at the beam waist. Second-harmonic light produced in the crystal exits the cavity via a dichroic mirror. The cavity is locked to the infrared laser using a standard technique [16]. The cavity enhancement is typically between 50 and 70, so that 3 mW of incident IR light results in roughly 0.5 μW of UV light at 377.6 nm. The bandwidth of the locking circuit is sufficient to keep the doubling cavity locked when we tune the infrared laser at rates up to 5 GHz/sec. Over the course of our typical UV scans of 50 GHz (25 GHz in the fundamental), the cavity locking and scanning circuitry must reacquire lock to a new bowtie cavity mode one or more times, producing very brief ''dropouts'' in the UV output, which must be processed and removed prior to data analysis. The entire optical system rests on a vibration-isolated optical table, although the stability of the doubling cavity remains quite sensitive to acoustical room noise, which we work to minimize.

The UV light exiting the cavity is incident on an optical chopper wheel which modulates the light at a frequency of roughly 1 kHz. Two identically constructed photomultiplier tubes [17] and preamplifier circuits are used to detect the UV light. 10% of the light is picked off and directed into one tube to provide the normalization signal. The balance of the UV light is directed into our vapor cell oven apparatus. Here, a 15-cm-long sealed quartz thallium cell is centered within a 1-m-long ceramic tube which is evacuated and then backfilled with 20–40 torr of helium gas. Using a variable duty-cycle temperature regulation scheme we hold the temperature of the cell near 400 °C with a long-term stability of better than 1 °C. At temperatures near this value, the thallium absorption in our cell corresponds to between one and four optical depths on the strongest ($F=1\rightarrow F'=1$) hyperfine transition. The light transmitted through the cell is directed into the second photomultiplier tube. The modulated UV laser signals from both the transmission and normalization detectors are analyzed in a pair of digital lock-in amplifiers (Stanford Research Systems SR810). A computer controls the voltage to a piezoelectric transducer (PZT) device which ramps the 755-nm laser frequency, and collects the output signals from the lock-in amplifiers, as well as the Fabry-Pérot transmission signals and a cell-temperature monitor.

III. DATA AND ANALYSIS

A single ~ 1 min scan consists of between 1000 and 2000 points taken over a (UV) frequency range of 40–60 GHz. We collect data for both increasing and decreasing laser frequency, and for different sweep speeds. In all, roughly 300 h individual scans were obtained over a several month period. Prior to data analysis, we determine the Fabry-Pérot cavity FSRs with the use of the wavemeter as described in Ref. [14]. Repeated measurements over the course of several weeks resulted in the values $\mathrm{FSR}_1 = 326.1(1)$ MHz and $\mathrm{FSR}_2 = 543.2(1)$ MHz. For the purposes of analysis of UV spectra with frequency-doubled light, we must multiply these values by 2. The first step in data analysis is to use one or the other set of Fabry-Pérot cavity transmission data to generate a mapping from point number to frequency, using a standard cubic spline interpolation technique. This procedure addresses both the absolute calibration as well as the linearization of the scan. The maximum nonlinearity of our scans never exceeded a few percent over their ~ 50 GHz extent. Previously [6,14] we have confirmed the consistency between the predictions of this interpolation technique and that based on a complete fit of the Fabry-Pérot data to an Airy function with frequency parametrized as a polynomial function of scan point number.

Vapor cell transmission data are divided by the normalization signal prior to analysis. This procedure removes both an overall frequency-dependent slope in the UV power output, as well as a large degree of the correlated short-term laser intensity fluctuations. However, the normalization does not leave us immune to brief UV ''dropouts'' due either to doubling-cavity instability or to the need for the cavity to recapture lock during the scans. These transients, typically lasting for 10 or 20 points out of the total ~ 1500 points, are tagged by inspection and analysis of the normalization data, and corresponding data points are assigned a very large uncertainty (and hence effectively ignored) in the subsequent fitting procedure.

In order to analyze our UV spectra, we have adapted a line shape fitting routine used previously for analysis of thallium vapor cell spectra [2,6]. A nonlinear least squares fitting routine [18] fits the frequency-linearized data to a sum of six Voigt profiles. The fitted values for the Gaussian component of the Voigt profiles are consistent with the measured cell temperature. The Lorentzian component reflects both the natural lifetime of the thallium $7S_{1/2}$ state as well as collisional broadening. From our measured widths, we estimate that roughly 50 torr of helium gas from the oven tube surrounding our quartz thallium cell has entered the cell at these elevated temperatures. Any possible collisional frequency *shift* in the hyperfine energy differences we measure is negligible compared to our final uncertainties.

The fitting routine incorporates known values for the isotopic abundances and relative line strengths of the six observed peaks. As mentioned, the relative line splittings are parametrized in terms of the ground- and excited-state HFS for each isotope as well as the transition isotope shift. The optical depth of the scan, defined as the number of absorption lengths on the strongest ^{205}Tl hyperfine peak, is also determined by the fitting routine. Figure 3 shows the normalized transmission data from a typical scan, as well as the results of the nonlinear least squares fit to the data. Analysis of a single scan such as this typically determines the various frequency splittings with statistical uncertainty of between 5 and 10 MHz.

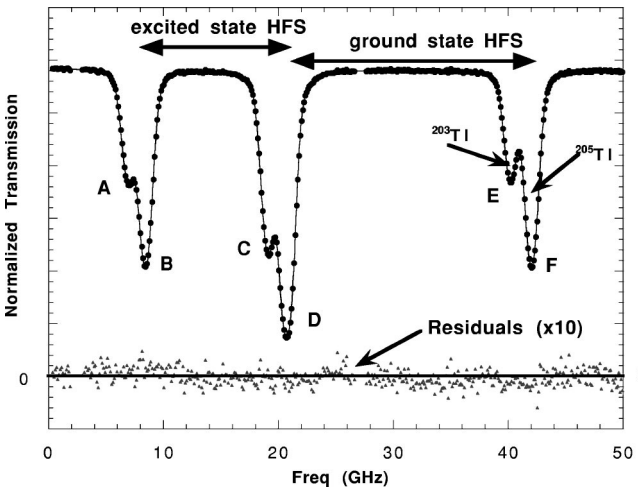

FIG. 3. Example of the normalized UV transmission data in the vicinity of the 378-nm transition. Data points as well as the results of our nonlinear least squares fit to the data (solid line) are shown. Displayed below, multiplied by a factor of 10, are the residuals of this fit. The letters labeling peaks refer to Fig. 1. Note the unequal frequency spacings between consecutive peaks. These splittings represent different combinations of the transition isotope shift and the isotopic differences in hyperfine splittings of ground and excited states. The two small gaps in the data reflect brief UV power drops caused by the doubling cavity momentarily losing lock.

IV. EXPLORATION OF SYSTEMATIC ERRORS

To explore the potential systematic error associated with both the frequency linearization and interpolation procedure, we generated frequency axis information independently from the two Fabry-Pérot cavities, and compared the results of the atomic line shape analysis based on each. There was less than 1 MHz systematic difference in fitted frequency splitting based on the two sets of Fabry-Pérot data, and the typical scan-to-scan variations were below the statistical errors in the frequency parameters as generated by the fit. Next, we explored the consistency between absolute frequency calibration as determined by the FSR measurements (FP calibration) and by the ground-state hyperfine splittings (atomic calibration) as follows. Initially, the frequency axis of each data set is determined by prior FP calibration. Note again that every thallium spectrum we collected includes as part of the scan the ground-state hyperfine splittings of the isotopes (see Fig. 3), whose values are known with sub part-per-million accuracy [7]. For the purposes of this systematic check, we then refit our data allowing the parameters corresponding to the ground-state HFS to be optimized simultaneously with the others. Any systematic discrepancy between the values derived from the fit and the accepted values of the ground-state splittings would thus signal an error in

the Fabry-Pérot FSR calibration used to generate the frequency axis. In that event, one can compute corrected values for all frequency parameters by simply scaling all measured frequency intervals by the ratio of known ground-state splittings to those extracted from the fit.

After averaging the results of many scans, we found that the discrepancy between fitted versus known values for the ground-state frequency splitting was roughly 2 MHz out of 21 GHz. This can be explained by a fractional error in Fabry-Pérot FSR calibration of 1 part in 10^4, which surpasses the quoted precision with which we determined the Fabry-Pérot FSRs. Thus, while the atomic and FP frequency calibration methods are consistent within our uncertainties, we ultimately chose to rely on the more precise atomic method for absolute frequency calibration. The Fabry-Pérot data were then used exclusively for frequency linearization and interpolation.

Results of data analysis for upward- and downward-going laser sweeps and for sweeps of varying width and speed were compared and generally found to be in agreement at the level of 1 MHz. A small subset of the data showed evidence of somewhat greater systematic differences related to sweep direction (of order 5 MHz). These runs were taken under fairly extreme laser sweep conditions, where the nonlinearity and hysteresis of the laser PZT would likely be most evident. Though *averaging* up and down sweeps for this subset of data reduced the magnitude of this systematic error substantially, these data were not used in the final frequency determinations. However, by studying the consistency of the average of up and down sweeps for this subset of data with that from the balance of our data, we were able to establish error estimates for this potential systematic error source.

We also explored the consistency of our fit results with respect to different data-weighting models. Data were fitted to a nominal ''flat weighting'' scheme, as well as a weighting determined by experimentally measuring the noise as a function of laser transmission. As can be seen in Fig. 3, in order to obtain a continuous scan across all hyperfine structure, there are substantial portions of the scan far from spectral peaks which could in principle be weighted much less in the fit. Thus we also employed a fitting scheme that emphasized only the data in the vicinity of each transmission peak. We found that the choice of data-weighting method influenced the fitted frequency values by no more than 0.3 MHz.

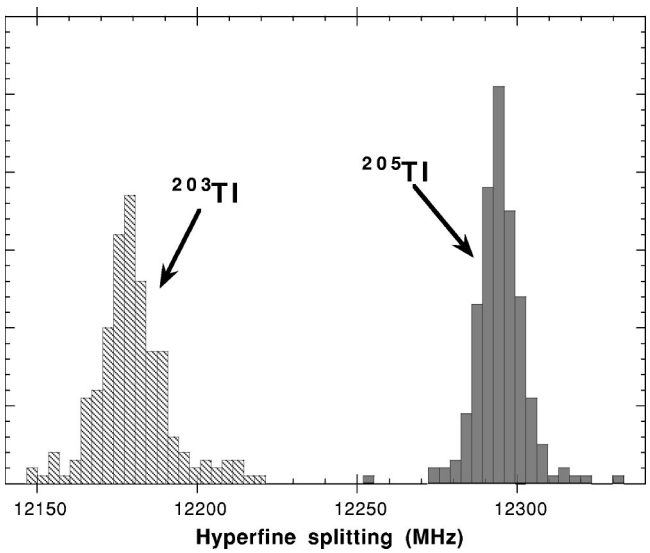

FIG. 4. Histograms of all measured values of the thallium 203 and 205 $7S_{1/2}$-state hyperfine splittings. The comparatively larger width of the 203 peak reflects its smaller isotopic abundance and the resulting smaller peak signal-to-noise ratio.

Finally, we studied our results as a function of vapor cell temperature. Over a range corresponding to a factor of 5 in thallium optical depth, we saw no significant dependence of measured frequency splittings on temperature. We note that certain systematic error sources (such as those associated with overall frequency calibration) would scale with the measured frequency interval, and thus result in smaller absolute frequency uncertainties for the much smaller IS interval as compared to the HFS splittings. Also, the presence of three pairs of 203-205 transmission peaks in each spectrum resulted in greater inherent precision for this measured frequency interval.

V. RESULTS AND DISCUSSION

Figure 4 shows histograms of all measurements of the $7S_{1/2}$-state hyperfine splittings for each isotope. Fitting these distributions to Gaussians results in center frequencies whose value and uncertainty agree well with those from other methods of analysis. Table I lists our final values and summarizes

TABLE I. Summary of results and contributions to the overall error in measured frequency intervals (see text).

	$7S_{1/2}$ (^{205}Tl) HFS	$7S_{1/2}$ (^{203}Tl) HFS	$6P_{1/2}$-$7S_{1/2}$ Transition IS
Final result (MHz)	12294.5	12180.5	1659.0
Statistical error (MHz)	0.5	0.8	0.3
Systematic error sources (MHz)			
Laser sweep (dir., speed, width)	1.0	1.0	0.2
Frequency linearization/interpolation	0.8	1.2	0.3
Fitting/data-weighting method	0.3	0.3	0.3
Thallium optical depth	0.2	0.2	0.2
Combined error total (MHz)	1.5	1.8	0.6

TABLE II. Summary of measurements of thallium $7S_{1/2}$-state splittings. All results are in MHz.

	^{205}Tl	^{203}Tl
Current results	12294.5(1.5)	12180.5(1.8)
Ref. [9]	12297.2(1.6)	12181.6(2.2)
Ref. [10]	12284.0(6.0)	12172.0(6.0)
Ref. [20]	12318(36)	12225(42)

the contributions to the total uncertainty of each measured frequency interval from statistical error as well as the sources of systematic error discussed above.

As can be seen in Table II, our hyperfine splitting measurements are in good agreement with, and of comparable precision to, the most recent measured values by Hermann *et al.* [9], in which they corrected errors in their earlier published work [8,21]. Our current values are in relatively poor agreement with the less precise 1985 measurements by Neugart *et al.* [10]. From our measured values of the hyperfine splittings A_{205} and A_{203}, we can deduce the hyperfine anomaly $\Delta \equiv [(A_{205}/A_{203})(g_{203}/g_{205})-1]$, where the g's refer to the nuclear g factor of the relevant isotope. Using precise values for the g factors tabulated in [19], we find that $\Delta = -4.7(1.5)\times 10^{-4}$. As shown in [12], this experimental quantity can be combined with nuclear structure calculations regarding the magnetic moment and charge distributions in the isotopes to infer a value for the mean square isotopic *change* in these distributions, referred to as $\lambda_{c,m}$ in [12]. We infer $\lambda_{c,m} = 0.61(20)$ fm^2 based on our experimental results and this theoretical model. The equivalent derivation based on the results for the $7S_{1/2}$-state HFS reported in [9] gives $\lambda_{c,m} = 0.45(24)$ fm^2. In both cases, the quoted uncertainty in λ reflects experimental errors only. Given these uncertainties, the $7S_{1/2}$ values are in good agreement with each other, and with the value for $\lambda_{c,m}$ derived from the (much more precise) ground-state hyperfine anomaly [7,12]: $\lambda_{c,m}(6P_{1/2}) = 0.42$ fm^2.

We turn finally to our result for the ^{205}Tl-^{203}Tl transition isotope shift [$\delta\nu_{205\text{-}203} = 1659.0(6)$ MHz]. Except for a measurement prior to the advent of lasers possessing a factor of 50 larger uncertainty [20], there has been no direct measurement of the isotope shift within this 378-nm transition. Using the value for the ground-state level isotope shift (LIS) relative to the ionization limit derived in [9] of $-1250.0(3.8)$ MHz, our result allows us to infer a value of $+409.0(3.8)$ MHz for the thallium $7S_{1/2}$-state LIS. This agrees well with the value for this LIS inferred from other transition isotope shift intervals also reported in [9]. Combining our result for the 378-nm transition with the precise measurement of the thallium $6P_{3/2}$-$7S_{1/2}$ 535-nm transition isotope shift [9], we can deduce the value of $\delta\nu_{205\text{-}203} = -98.3(7)$ MHz for the TIS of the thallium 1283-nm $6P_{1/2}$-$6P_{3/2}$ $M1$ transition. Direct measurement of this TIS is difficult due to the forbidden nature of this transition and its intrinsically small size. Yet accurate knowledge of its magnitude is essential given the importance of this transition to current and future measurements of parity nonconservation in thallium [2,6].

VI. CONCLUDING REMARKS

In summary, we have used a laser diode and external frequency-doubling cavity to generate a small amount of tunable UV light near 378 nm. With this source, we have measured the excited $7S_{1/2}$-state hyperfine splittings in the stable thallium isotopes. At the same time we have made a greatly improved measurement of the isotope shift within this transition. This laser system will next be used in conjunction with an atomic beam apparatus recently constructed in our laboratory to complete a precise Stark-shift measurement within the $6P_{1/2}$-$7S_{1/2}$ transition. Here, the diode laser will be locked to a stable reference cavity, and its frequency tuned via an acousto-optic modulator prior to frequency doubling. We will then study the Doppler-narrowed transmission spectrum of the UV light as it interacts with the atomic beam in the presence of a large, precisely calibrated electric field.

ACKNOWLEDGMENTS

We would like to thank Leo Tsai and Peter Nicholas for help at an early stage of this experiment, and Andrew Speck for aid in data acquisition and analysis. We gratefully acknowledge the support of the National Science Foundation through the RUI program (Grant No. 9721403) and the MRI program (Grant No. 9724246).

[1] C. S. Wood, S. C. Bennett, D. Cho, B. P. Masterson, J. L. Roberts, C. E. Tanner, and C. E. Wieman, Science **275**, 1759 (1997).
[2] P. A. Vetter, D. M. Meekhof, P. K. Majumder, S. K. Lamoreaux, and E. N. Fortson, Phys. Rev. Lett. **74**, 2658 (1995).
[3] S. A. Blundell, W. R. Johnson, and J. Sapirstein, Phys. Rev. Lett. **65**, 1411 (1990).
[4] V. A. Dzuba, V. V. Flambaum, P. G. Silvestrov, and O. P. Sushkov, J. Phys. B **20**, 3297 (1987).
[5] S. G. Porsev (private communication).
[6] P. K. Majumder and Leo L. Tsai, Phys. Rev. A **60**, 267 (1999).
[7] A. Lurio and A. G. Prodell, Phys. Rev. **101**, 79 (1956).
[8] G. Hermann *et al.*, Phys. Lett. A **151**, 69 (1990).
[9] G. Hermann *et al.*, Z. Phys. D: At., Mol. Clusters **28**, 127 (1993).
[10] R. Neugart *et al.*, Phys. Rev. Lett. **55**, 1559 (1985).
[11] A. M. Martensson-Pendrill and A. C. Hartley, J. Phys. B **24**, 1193 (1991).
[12] A. M. Martensson-Pendrill, Phys. Rev. Lett. **74**, 2184 (1995).
[13] E. D. Commins *et al.*, Phys. Rev. A **50**, 2960 (1994).
[14] P. C. Nicholas and P. K. Majumder (unpublished).
[15] Wavetrain-CW model, manufactured by Laser Analytical Systems, GmBH.
[16] T. W. Hansch and B. Couillard, Opt. Commun. **35**, 441 (1980).

[17] Hamamatsu Model R1529. See P. Mitchell, Laser Focus World **28**, (Jan. 1992), for discussion of the improved linearity of the Cockroft-Walton dy- node chain employed in this device.
[18] W. H. Press *et al.*, *Numerical Recipes* (Cambridge University Press, Cambridge, England, 1986).
[19] P. Raghavan, At. Data Nucl. Data Tables **42**, 189 (1987).
[20] C. J. Shuler *et al.*, J. Opt. Soc. Am. **52**, 501 (1962).
[21] M. Grexa *et al.*, Phys. Rev. A **38**, 1263 (1988).